

# SYNTHESIS, CHARACTERIZATION OF $Mn_3O_4$ : ADSORPTION APPLICATION AND ANTIBACTERIAL EVALUATION

AMAINI CHOUCHAINE<sup>1</sup>, IKHLASS MARZOUK TRIFI<sup>2\*</sup>, BEYRAM TRIFI<sup>3</sup>, OUASSIM GHODBANE<sup>4</sup>,  
HASSOUNA DHAOUADI<sup>3</sup>, FATHI TOUATI<sup>3</sup>, NOUREDDINE AMDOUNI<sup>1</sup> AND SALAH KOUASS<sup>4</sup>

<sup>1</sup>Université de Tunis El Manar, Faculté des Sciences de Tunis, Laboratoire de Caractérisation Applications et Modélisation de matériaux, Campus Universitaire El Manar, Tunis, 2092, Tunisie

<sup>2</sup>Université de Tunis El Manar, Faculté des Sciences de Tunis, Laboratoire Dessalement et Traitement des Eaux, Campus Universitaire El Manar, Tunis, 2092, Tunisie

<sup>3</sup>Institut National de Recherche et d'Analyse Physico-chimique (INRAP), Laboratoire Matériaux Traitement et Analyse, Sidi Thabet, 2020, Tunisie.

<sup>4</sup>Institut National de Recherche et d'Analyse Physico-chimique (INRAP), Laboratoire Matériaux Utiles Sidi Thabet, 2020, Tunisie.

## ABSTRACT

$Mn_3O_4$  were synthesized via the hydrothermal method at 200°C for 24 h, using surfactants. The resultant products were examined by powder X-ray diffraction (XRD), Raman spectroscopy, Fourier transform infrared spectroscopy (FTIR), transmission electronic microscope (TEM), UV-visible spectroscopy and BET surface area analysis. The as-prepared materials were used for the adsorption of methylene blue dye (MB). The effect of various experimental parameters (initial concentration, adsorbent dose and temperature) and optimal experimental conditions were ascertained by response surface methodology using Doehlert model. Finally, the antibacterial activity of  $Mn_3O_4$  nanoparticles was tested.

**Keywords:** Synthesis; Characterization;  $Mn_3O_4$ ; Methylene blue; Adsorption; Antibacterial activity.

## 1. INTRODUCTION

Transition metal oxides are important for the development of new materials with unique physical and chemical properties [1,2]. In particular Manganese oxides has attracted considerable interest due to their outstanding structural flexibility which provide wide-spread applications in catalysts [3-5], batteries [6-8], supercapacitors magnetic materials [9-11] and in wastewater treatment [12,13]. The protection of the environment and natural resources is a serious problem for humanity. The increase in industrial activities is putting increasing pressure on freshwater supplies. Indeed, many industries (textiles, stationery, cosmetics, food ...) are large consumers of water and use organic dyes. These dyes are both toxic and responsible for coloring water. They can accumulate in organisms and present risks to our health and nuisance to the environment [14-16]. The treatment of these pollutants has been investigated by using several processes such as biodegradation [17-20], chemical and oxidative process [21-26], or physicochemical processes [27-30]. Among these processes, adsorption is considered as an effective technique that has already shown its potential and has become a method of choice due to the initial cost, the simplicity of design, the ease of use and the insensitivity to toxic substances [31,32]. Thus, several types of adsorbents have been used to remove dyes such as clay minerals [33,34], carbon-based materials [35-37], and metal oxides [38,39]. Owing to the high surface charge density and the high sorption capacity, various Mn oxides (e.g., including pyrolusite ( $-MnO_2$ ) and birnessite ( $-MnO_2$ )) have been extensively used as high efficient adsorbents to remove dyes [40-43].

Furthermore, it's be noted that many research has been focused on the synthesis of novel inorganic antibacterial reagents [44,45]. Indeed, many works on nanomaterials based on transition metal oxides such as MgO, ZnO and TiO<sub>2</sub> have been reported in this area [46-48]. Among them, nanocrystalline magnetite has proved to be an effective antimicrobial agent. This depends principally on the nanoparticle's characteristics, such as size and the morphology

In this paper, we described the hydrothermal synthesis of  $Mn_3O_4$  nanomaterials. The application of this oxide was investigated for the removal of Methylene blue via Response Surface Methodology (RSM) approach in order to determine the optimal condition of adsorption. The evaluation of antibacterial activity of the as-prepared oxide was also investigated.

## 2. EXPERIMENTAL

A known quantity of manganese chloride  $MnCl_2 \cdot 4H_2O$  ( $\geq 99\%$ ), as metal precursor and Polyethylene glycol (PEG), TRITON X100 and Sodium dodecyl sulfate (SDS) as surfactant was chosen in protocol. The synthesis of nanoparticles  $Mn_3O_4$  was carried out using hydrothermal route. At first, 0.591g of  $MnCl_2 \cdot 4H_2O$  was dissolved in 5 mL of distilled water subjected to magnetic stirring at room temperature.

In the second step, 5 ml of NaOH solution was added and continuously stirred for 1 h. This mixture was transferred in to a stainless-steel autoclave, which was heated to 200°C and maintained for 24 h and then cooled to room temperature. The products recovered after filtration are washed with water and ethanol several times to remove the organic compounds and then dried at 300 °C for 2 hours.

XRD measurements were carried out with a Panalytical XPERT PRO MPD diffractometer operating with  $CuK\alpha$  radiation. The morphologies were characterized using an FEI Quanta 200 environmental scanning electron microscope. Infrared spectra (IR) spectra were taken using a "Nicolet 380 Spectrometer" instrument in the range from 4000 to 400  $cm^{-1}$ . Raman spectra of  $Mn_3O_4$ doped were recorded with the INVIA confocal micro Raman spectrometer (RENISHAW) equipped with a CCD detector. Spectral resolution of the Raman spectrometer was 1-2  $cm^{-1}$ , the measurement frequency range is in 100–1500  $cm^{-1}$ . Optical absorption spectra of the sol were recorded on an ultraviolet–visible (UV–vis) spectrophotometer (Shimadzu UV3101PC) between wave length of 300 and 800 nm.

## 3. RESULTS AND DISCUSSION

### 3.1 Structure analysis

The nanoparticles of  $Mn_3O_4$  compound obtained by hydrothermal method were characterized by X-ray diffraction. All of the XRD peaks in the Fig.1 can be readily indexed to a tetragonal Hausmannite phase of  $Mn_3O_4$  (space group I41/and with lattice constant  $a = b = 5,7621\text{Å}$  and  $c = 9,4696\text{Å}$ .) [49]. No obvious peaks of impurities were found. Then, it could be concluded that  $Mn_3O_4$  with high purity can be obtained via the hydrothermal treatment at 200°C for 24 hours.

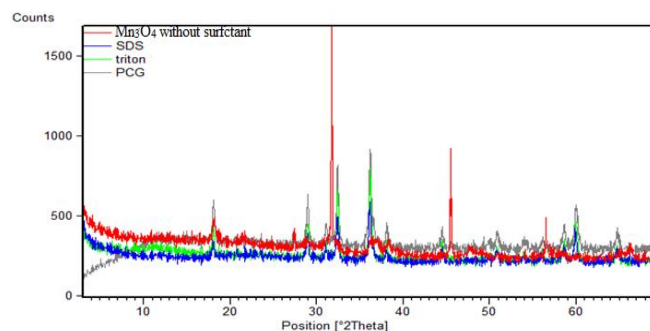


**Figure 1:** X-rays diffraction patterns of  $Mn_3O_4$  with different surfactants (SDS, Tritonx 100 and PEG 300)

The average crystallite size of the synthesized  $Mn_3O_4$  powders, mineralogical name hausmannite [50], was calculated from Scherrer formula using the equation (1) and the results are given in Table 1:

$$d = k\lambda/(\beta \cos \theta) \quad (1)$$

**Table 1:** Crystallite size,  $S_{BET}$  and  $E_g$  of  $Mn_3O_4$  nanomaterials

Samples	Crystallite size D (nm)	$S_{BET}$ ( $m^2 g^{-1}$ )	$E_g$ (eV)
witness	86	7.5591	1.97
Triton X-100	82	8.8918	1.98
PEG 3000	50	12.5623	2.02
SDS	40	21.5244	2.08

### 3.2 Morphological studies

The morphology of the particles was also examined by direct observation via TEM. The TEM micrographs for samples are given in Fig. 2.

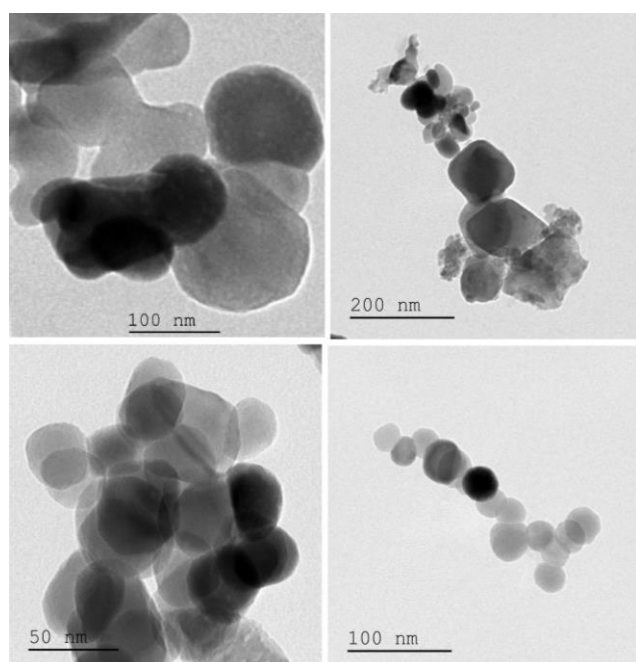


**Figure 2:** TEM images of products synthesized by hydrothermal of oxide of manganese  $Mn_3O_4$ : (a) without surfactants, (b) With SDS, (c) With PEG 3000, (d) With TRITON X 100

The morphology of the nanostructured  $Mn_3O_4$  powder can be changed by using surfactants. Three distinct morphologies are observed: the first one consists of nanoplatelet particles corresponding to the  $Mn_3O_4$  phase, without surfactants and with PEG, their size are 90 and 50 nm respectively (Fig. 2a and Fig. 2c). Second morphology of the  $Mn_3O_4$  powder using TRITON X 100 is shape with a 80 nm in length, can be seen in Fig. 2b.

However, Fig. 2d shows spherical shape of  $Mn_3O_4$  using SDS with a uniform diameter of 40 nm and smooth surfaces. The TEM images also show that the size of the nanoparticles decreases of 90 to 40 nm without and using TRITON X, PEG and SDS respectively. Thus, the surfactants may influence the size and morphology of  $Mn_3O_4$  by its involvement in the nucleation and growth.

### 3.3 IR and Raman spectroscopy

#### 3.3.a. FTIR analysis

FTIR analysis was carried out to confirm the chemical nature of the as-made nanomaterials also improve the presence of phase of  $Mn_3O_4$  prepared at 200°C for 24 hours recorded in the region 400–4000  $cm^{-1}$ . The FTIR spectra of manganese oxide  $Mn_3O_4$  with three surfactants (SDS, PEG 3000 and TRITON X 100) are illustrated in Fig. 3.

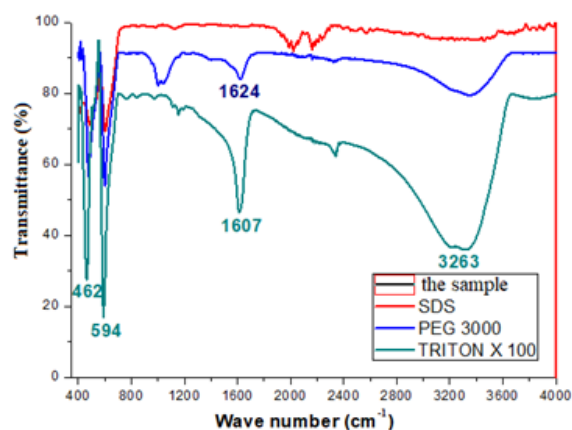


**Figure 3:** IR spectra of  $Mn_3O_4$  nanoparticles with different surfactants (SDS, Triton X-100 and PEG 3000)

The peak situated at 594  $cm^{-1}$  is assigned to the stretching mode Mn-O ( $A_{1g}$  mode) of manganese oxide of  $Mn^{2+}$  ions at tetrahedral sites [51]. Whereas, the other peak located at 462  $cm^{-1}$  represent the doubly degenerate  $T_{2g}$  symmetry mode, which is reliable with the tetragonal structure of  $Mn_3O_4$  [51]. The band centered at 1600  $cm^{-1}$  can be attributed to the stretching and bending of O–H group [52]. Moreover, the broad band observed at 3263  $cm^{-1}$  indicates the stretching vibrations of  $H_2O$  molecules on the surface of samples [52]. This result is in a good agreement with X-ray diffraction data to confirm that the synthesized compound was  $Mn_3O_4$ .

#### 3.3.b. Raman Spectroscopy

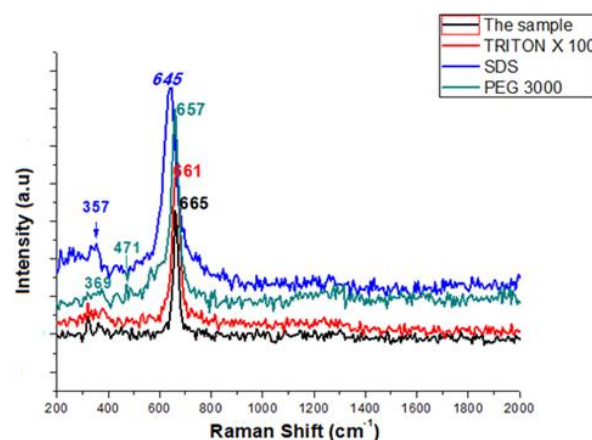


**Figure 4:** Raman spectra of tetragonal hausmannite  $Mn_3O_4$  powder with surfactants (SDS, Triton X 100 and PEG 3000).

Figure 4 shows the Raman spectra of  $Mn_3O_4$  nanoparticles recorded in the range 100–4000  $cm^{-1}$ . Raman spectra of the different samples were similar during adding of surfactant and were presented in the inset of figure. The intense peak at 657  $cm^{-1}$  corresponding to attributed to stretching mode ( $A_{1g}$  mode) of manganese oxide in  $Mn^{2+}$  ions at tetrahedral site [53] and two small peaks at 368  $cm^{-1}$  and 470  $cm^{-1}$  represent the doubly degenerate  $T_{2g}$  symmetry mode [54] which is reliable with the tetragonal structure of  $Mn_3O_4$ [55,56].

#### 3.4 Optical properties

Optical studies were carried out to investigate the effect of adding surfactants to the oxide of manganese in the range of wavelength 200–800 nm. The optical band gap of manganese oxide has been estimated using a Tauc plot given in Fig. 5, and the equation below.

$$(ah\nu) = B(h\nu - E_g)^n \quad (2)$$

Where B is a constant,  $h\nu$  is the photon energy,  $E_g$  is the optical bandgap energy and n is equal to 2 or 1/2 depending upon the type of transition (direct or indirect transition).

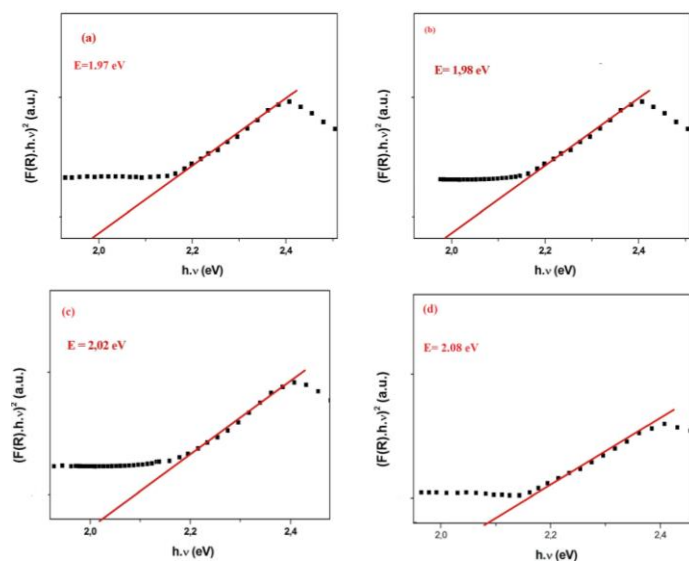


**Figure 5:** Plot of  $[\alpha \cdot h\nu]^2$  versus  $h\nu$ .

Tauc's plot is drawn by plotting the photon energy  $h\nu$  (eV) versus  $(\alpha h\nu)^2$  and then extrapolating the linear portion to the x-axis for  $(\alpha h\nu)^2 = 0$  [57]. Such plots for samples of manganese oxide with surfactants are shown in Fig. 5, respectively.

Eg values of all the  $\text{Mn}_3\text{O}_4$ ,  $\text{Mn}_3\text{O}_4/\text{Triton}$ ,  $\text{Mn}_3\text{O}_4/\text{PEG 3000}$  and  $\text{Mn}_3\text{O}_4/\text{SDS}$  are shown in Table 1. The determined energy gap values are 1.97, 1.98, 2.02 and 2.08 eV for  $\text{Mn}_3\text{O}_4$ ,  $\text{Mn}_3\text{O}_4/\text{Triton}$ ,  $\text{Mn}_3\text{O}_4/\text{PEG 3000}$  and  $\text{Mn}_3\text{O}_4/\text{SDS}$  respectively. The gap Eg energies of the materials elaborated with the  $\text{Mn}_3\text{O}_4$  and  $\text{Mn}_3\text{O}_4/\text{Triton}$  are very close. The low difference in energy gap values elaborated is related to average size of the crystallites. The material synthesized with the SDS has gap energy greater than the others. They are in agreement with those reported in the literature for  $\text{Mn}_3\text{O}_4$  nanoparticle [58]. The value band gap of the samples near 1.4 eV, classifies the corresponding materials among the semiconductors.

### 3.5. Adsorption capacity

#### 3.5.a. Surfactant effect

In this study, the removal of MB is considered by adsorption onto oxide of manganese synthesized with surfactants: SDS, PEG 3000 and TRITON X 100 respectively. The adsorption study was carried out with in initial dye concentration  $5 \text{ mg L}^{-1}$ , and 5 mg in 10 mL of  $\text{Mn}_3\text{O}_4$ . The results are presented in Fig. 6.

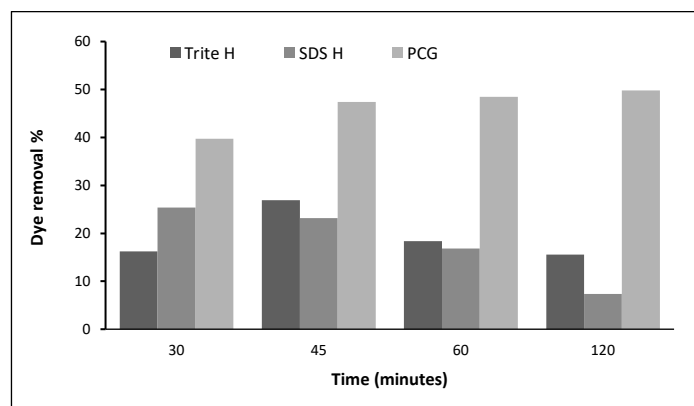


**Figure 6:** Effect of surfactant on dye removal.

Results show that the adsorbent synthesized with the surfactant PEG 3000 allows to reach the best dye removal efficiency,  $\approx 50\%$ . However, with SDS and Triton, the adsorption rates remain lower than to PEG. Thus, in the remainder of this study, the adsorbent synthesized with PEG will be chosen.

### 3.5b. Doehlert Design

The Response Surface Methodology via Doehlert design was employed to optimize experimental parameters. In fact, RSM is more economical and efficient than the traditional "one at a time" method, thus saving time by greatly reducing the number of experiments and thereby facilitating the determination of optimal light conditions for interaction between the experimental parameters [59-61]. For the Doehlert matrix, which makes it possible to estimate the coefficients of a second order function and which is also capable of predicting, at any point in the experimental field the values of the response (Y), the number of experiments for k factors is:

$$N = k^2 + k + 1 \quad (3)$$

The mathematical relation of the responses Y is:

$$Y = b_0 + b_1 X_1 + b_2 X_2 + b_3 X_3 + b_{11} X_1^2 + b_{22} X_2^2 + b_{33} X_3^2 + b_{12} X_1 X_2 + b_{13} X_1 X_3 + b_{23} X_2 X_3 \quad (4)$$

Where  $b_0$ ,  $b_1$ ,  $b_2$  and  $b_3$  are linear coefficients;  $b_{11}$ ,  $b_{22}$  and  $b_{33}$  are squared coefficients;  $b_{12}$ ,  $b_{13}$  and  $b_{23}$  are the second-order interaction terms and  $X_1$ ,  $X_2$  and  $X_3$  are the dimensionless coded factors of the experimental parameters studied pH, adsorbent dose and the temperature respectively. The experimental domain chosen is illustrated in table 2.

**Table 2 :** Experimental values and coded levels of factors variables

Coded values of the variables	Variables	-1 (Low)	0	+1 (High)
$X_1$ : D	U1 : Adsorbent dose	5	10	15
$X_2$ : [MB]	U2 : Concentration of MB	5	12.5	20
$X_3$ : T	U3 : Temperature	10	25	40

Doehlert design and experimental matrix are presented in the table 3.

**Table 3:** Experimental and design matrix

N°	Doehlert design matrix			Experimental matrix			Dyeremoval percentage	
	$X_1$	$X_2$	$X_3$	U1	U2	U3	Y Experimental	Y Predicted
1	1	0	0	15	12,5	25	46,4	48,1
2	-1	0	0	5	12,5	25	35,8	34,2
3	0.5	0.866	0	12,5	19,0	25	36,4	36,2
4	-0.5	-0.866	0	7,5	6,0	25	58,0	58,2
5	0.5	-0.866	0	12,5	6,0	25	69,0	67,9
6	-0.5	0.866	0	7,5	19,0	25	30,9	32,0
7	0.5	0.287	0.816	12,5	14,7	37,24	53,8	52,4
8	-0.5	-0.287	-0.816	7,5	10,3	12,76	33,3	34,7
9	0.5	-0.287	-0.816	12,5	10,3	12,76	42,8	42,2
10	0	0.577	-0.816	10	16,8	12,76	33,3	32,4
11	-0.5	0.287	0.816	7,5	14,7	37,24	45,4	46,0
12	0	-0.577	0.816	10	8,2	37,24	71,2	72,1
13	0	0	0	10	12,5	25	42,1	42,1

$$R^2=0.993.$$

Based on the experimental result ( $Y_{\text{Experimental}}$ ), the polynomial equation of the second order will be determined, allowing calculating the theoretical response ( $Y_{\text{Predicted}}$ ) for each experiment

$$Y_{\text{Predicted}} = 42.1 + 6.95 X_1 - 16.73 X_2 + 12.45 X_3 - 1 X_1^2 + 8.97 X_2^2 + 4.81 X_3^2 - 3.18 X_1 X_2 + 0.45 X_1 X_3 - 8.39 X_2 X_3 \quad (5)$$

This model presents a good agreement among the model's predicted values and the experimental values ( $R^2 = 0.993$ ).

To better interpret these results, we used Pareto analysis (Fig. 7) that is based on the calculation of the percentage of the effect of each factor (bi) on the response according to the following relation.

$$P_i = \left( \frac{b_i^2}{\sum b_j^2} \right) \times 100 \quad (6)$$

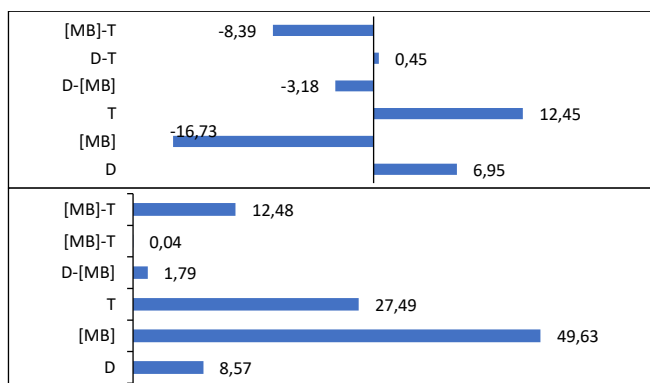


**Figure 7:** Effect of factors and their interactions (a) and Pareto analysis(b).

Fig. 7 (a) shows effects of factors and their interactions. It can be seen that the concentration of dye has a negative effect ( $b_2 = -16.73$ ) on the adsorption of MB; this implies that an increase in the concentration leads to a decrease in the percentage of elimination of MB. Moreover, the adsorbent dose ( $b_1 = +6.95$ ) and the temperature ( $b_3 = +12.45$ ) have a positive effect on the removal of MB so an increase in these factors implies an increase of the dye removal percentage. The effect of the adsorbent dose-temperature interaction is a significant interaction with a negative effect on adsorption of MB.

The graphical analysis of the figure 7 (b) shows that the concentration of the dye and the temperature are the most determining factors, their effect on the response studied is 49.63% and 27.49% respectively. Furthermore, the interaction between these two factors is the most important (12.48%). Thus, these two factors as well as their interaction provide more than 89% on the response. However, the adsorbent dose and the other interactions have a negligible effect; they represent only 10% of the studied response.

In order to find the optimal conditions for the reaction a response surface model was established by using NEMRODW® program. The optimum of each factor is dose = 11.1 g, initial concentration of Methylene blue 6.44 mg L<sup>-1</sup> and a temperature = 33.34 °C for 75.52 % efficiency of MB removal by adsorption onto Mn<sub>3</sub>O<sub>4</sub>.

In order to study the reproducibility of the optimized adsorption process, MB's adsorption was carried out 3 times under optimal conditions. The repetition of the adsorption of methylene blue leads to an average equal to 75.4 % and a CV<sub>R</sub> ≈ 1%. This reproducibility coefficient is less than 5 %, so the optimized adsorption process is considered reproducible.

### 3.7 Antibacterial activity

Fig. 8 shows the zone diameter of inhibition observed for magnetite and the control Ampicillin/Nystatine.

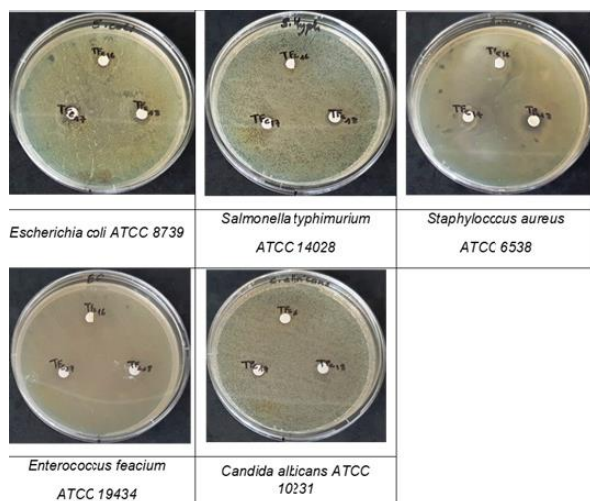


**Figure 8:** Diameter zone growth inhibition of magnetite nanomaterials.

The diameters of the zone of growth inhibition of the studied bacteria strains are summarized in Table 4.

**Table 4:** Antibacterial activity of magnetite nanomaterials.

Bacterial strain name by Disk load (μg)	Inhibition diameter (mm)			
	Ampicillin/Nystatine	TFe16 (pure)	TFe17 (CTAB)	TFe18 (SDS)
Escherichia coli ATCC 8739 G(-)	10μg per 100μg	15μg	15μg	15μg
Salmonella typhimurium ATCC 14028 G(-)	11,75±0.3	9.5±0.7	10.5±0.7	10.75±0.35
Staphylococcus aureus ATCC 6538 G(+)	13,75±1.0	7.25±0.3	8.5±0.7	8.5±0.7
Enterococcus faecium ATCC 19434 G(+)	35,5±0.7	-	-	-
Candida albicans ATCC 10231	27,5±0.7	-	-	-
	26±0.3	7.0±0.3	7.25±0.0	7.75±0.3

The results demonstrate that the antibacterial activity of the Mn<sub>3</sub>O<sub>4</sub> nanomaterials against (*Escherichia coli* ATCC 8739 G(-) and *Salmonella typhimurium* ATCC 14028 G(-)) is comparable to that observed for the control Ampicillin showing an important antibacterial activity. Whereas, the antibacterial efficiency of Mn<sub>3</sub>O<sub>4</sub> with different surfactant against the bacterial growth (*Candida albicans* ATCC 10231) is lower than that of the control sample, indicating a moderate antibacterial activity. The oxidative stress caused by ROS is the central mechanism responsible for the antibacterial activity of the particles [62, 63]. The iron oxide could produce the ROS ((O<sub>2</sub>·), (-OH), (H<sub>2</sub>O<sub>2</sub>) and (O<sub>2</sub>)), leading to the inhibition of the bacteria, hydrogen peroxide (H<sub>2</sub>O<sub>2</sub>) was generated when Fe responded with oxygen [64]. By evaluating the effects of particle size on the antibacterial activity of magnetite, we remark that the antibacterial activity of Mn<sub>3</sub>O<sub>4</sub> nanoparticles increased slightly when the size of particles decreases, showing the enhanced antimicrobial activity.

### CONCLUSION

This study reports the synthesis of Mn<sub>3</sub>O<sub>4</sub> using the hydrothermal route. By varying surfactants parameter, we have obtained manganese oxide with different morphologies. These materials were characterized by X-ray powder diffraction, Infrared spectroscopy, Scanning Electron Microscopy and UV-vis. The as-prepared materials were used for the adsorption of methylene blue dye (MB). Manganese oxide synthesized using PEG is the best adsorbent. The optimum of each factor is dose = 11.1 g, initial concentration of Methylene blue 6.44 mg L<sup>-1</sup> and a temperature = 33.34°C for 75.52 % efficiency of MB removal by manganese oxide. The antimicrobial studies reveal that magnetite nanomaterials constitute an effective antibacterial agent.

### REFERENCES

- Shen Y F, Zerger R P, DeGuzman R N, Suib S L, McCurdy L, Potter D I and O'Young C L 1993 *Science* **260** 511.
- Seo W S, Jo H H, K Lee, B Kim, Oh S J and Park J T 2004 *Angew. Chem. Int. Ed.* **43** 1115.
- Grootendorst E J, Verbeek Y and Ponc V 1995 *J. Catal.* **157** 706.
- Zhang L, Sun Z, Yao Z, Yang L, Yan N, Lu X, Xiao B, Zhu X and Chen L 2020 *Nanoscale Adv.* **2** 1666.
- Yinniana L, Xuana Z, Ruosi P, Mengqi Z and Daiqi Y 2017 *Appl. Surf. Sci.* **405** 20.
- Gao J, Lowe A M and Abruña H D 2011 *Chem. Mater.* **23** 3223.
- Cai Z, Xu L, Yan M, Han C, He L, Hercule K M, Niu C, Yuan Z, Xu W, Qu L, Zhao K and Mai L 2015 *Nano. Lett.* **15** 738.
- Bruce P G and Armstrong A R 1996 *Nature* **381** 499.
- Nagamuthu S, Vijayakumar S and Muralidharan G 2013 *Energy Fuels* **27** 3508.
- Radich J G, McGinn P J and Kamat P V 2011 *Electrochem. Soc. Interface* **20** 63.
- Bao S, Jia W and Xu M 2011 *Rare Met.* **30** 81.
- Zhang P, Zhan Y, Cai B, Hao C, Wang J, Liu C, Meng Z, Yin Z and Chen Q 2010 *Nano Res.* **3** 235.
- Bai Z, Sun B, Fan N, Ju Z, Li M, Xu L and Qian Y 2012 *Chem. Eur. J.* **18** 5319.
- Zheng T, Holford T R, Mayne S T, Owens P H, Boyle P and Zhang B 2002 *Eur. J. Cancer* **38** 1647.

15. Tezcanli-Guyer G and Ince N H 2003 *Ultrason. Sonochem.* **10** 235.
16. Sauer T, Neto G C, José H J and Moreira R F P M 2002 *J. Photochem. Photobiol Chem.* **149** 147.
17. Hazrat A 2010 *Water Air Soil Pollut.* **213** 251.
18. Joshi P A, Jaybhaye S and Mhatre K 2015 *Eur. J. Exp. Bio.* **5** 36.
19. Lade H, Kadam A, Paul D and Govindwar S 2015 *Exp. Clin. Sci. J.* **14** 158.
20. López-Grimau V, Vilaseca M and Gutiérrez-Bouzán C 2016 *Desalination Water Treat.* **57** 2685.
21. Trifi B, Cavadias S and Bellakhal N 2011 *Desalination Water Treat.* **25** 65.
22. Chianeh F N and Parsa J B 2016 *Desalination Water Treat.* **57** 20574.
23. Oturan M A and Aaron J J 2014 *Crit. Rev. Env. Sci. Technol.* **44** 2577.
24. Yang W, Zhou H and Cicek N 2014 *Crit. Rev. Env. Sci. Technol.* **44** 1443.
25. Kosa S A, Al-sebaili N M, Abd El Maksod I H and Hegazy E Z 2016 *J. Chem.* **2016** 1.
26. Garg V K 2015 *Green Process. Synth.* **4** 507.
27. Bazrafshan E, Alipour M R and Mahvi A H 2016 *Desalination Water Treat.* **57** 9203.
28. Gadekar M R and Ahammed M M 2016 *Desalination Water Treat.* **57** 26392.
29. Thamaraiselvan C and Noel M 2015 *Crit. Rev. Env. Sci. Technol.* **45** 1007.
30. Goh P S, Ng B C, Lau W J and Ismail A F 2015 *Sep. Purif. Rev.* **44** 216.
31. Sun Y B, Yang S B, Chen Y, Ding C C, Cheng W C and Wang X K 2015 *Environ. Sci. Technol.* **49** 4255.
32. Niu Y, Qu R, Sun C, Wang C, Chen H, Ji C, Zhang Y, Shao X and Bu F 2013 *J. Hazard. Mater.* **244** 276.
33. Adeyemo A A, Adeoye I O and Bello O S 2017 *Appl Water Sci.* **7** 543.
34. Ngulube T, Gumbo J R, Masindi V and Maity A 2017 *J. Environ. Manage.* **191** 35.
35. Yagub M T, Sen T K, Afroze S and Ang H M 2014 *Adv. Colloid Interface Sci.* **209** 172.
36. Zhou Y, Zhang L and Cheng Z 2015 *J. Mol. Liq.* **212** 739.
37. Trifi B, Bouallegue M C, Marzouk Trifi I 2019 *Desalination Water Treat.* **154** 369.
38. Li L H, Xiao J, Liu P and Yang G W 2015 *Sci. Rep.* **9028** 1.
39. Jethave G, Fegade U, Rathod R and Pawar J 2018 *J. Dispers. Sci. Technol.* **40** 563.
40. Karaseva O N, Ivanova L I and Lakshtanov L Z 2019 *Geochem. Int.* **64** 1091.
41. Liu Z, Zhong X, Wang Y, Ding Z, Wang C, Wang G and Liao S 2018 *Arab. J. Sci. Eng.* **43** 2155.
42. Zou W, Zhang J, Li K, Han P and Han R 2009 *Adsorpt. Sci. Technol.* **27** 549.
43. Huang X, Chen T, Zou X, Zhu M, Chen D and Pan M 2017 *Int. J. Environ. Res. Public Health* **14** 1.
44. Wang X J, Qiao X L, Chen J G, Wang H S and Ding S Y 2003 *J. Ceram.* **24** 39.
45. Fang M, Chen J H, Xu X L, Yang P H and Hildebrand H F 2006 *Int. J. Anti-microb. Agents* **27** 513.
46. Makhluif S, Dror R, Nitzan Y, Abramovich Y, Jelinek R and Gedanken A 2005 *Adv. Funct. Mater.* **15** 1708.
47. Ghule K, Ghule A V, Chen B J and Ling Y C 2006 *Green Chem.* **8** 1034.
48. Daoud W A, Xin J H and Zhang Y H 2005 *Surf. Sci.* **599** 69.
49. Laffonta L and Gibotb P 2010 *Mater. Charact.* **61** 1268.
50. Augustin M, Fenske D, Bardenhagen I, Westphal A, Knipper M, Plaggenborg T, Joan K O and Jürgen P 2015 *Beilstein J. Nanotechnol.* **6** 47.
51. Salavati-Niasari M, Davar F and Mazaheri M 2008 *Polyhedron.* **27** 3467.
52. Nâamoune F, Messaoudi B, Kahoul A, Cherchour N, Pailleret A and Takenouti H 2012 *Ionics* **18** 365.
53. Gnana B, Raj S, Asiri A M, Wu J J and Anandan S 2015 *J. Alloys Compd.* **636** 234.
54. Buciuman F, Patcas F, Craciun R and Zahn D R T 1999 *Phys. Chem. Chem. Phys.* **1** 185.
55. Mironova-Ulmanea N, Kuzmina A and Grube M 2009 *J. Alloys Compd.* **480** 97.
56. Hu Y, Chen J and Xue X 2006 *Mater. Lett.* **60** 383.
57. Kuang L, Dong R, Zhang Z, Feng L, Wang F and Wen Y 2013 *Mater. Res. Bull.* **48** 3122.
58. Dubal D P, Dhawale D S, Salunkhe R R, Fulari V J and Lokhande C D 2010 *J. Alloys Compd.* **497** 166.
59. Marzouk Trifi I, Trifi B, Ben Souissi E and Hamrouni B 2020 *Environ. Technol.* **41** 3473.
60. Trifi I M, Trifi B, Djemal A and Hamrouni B 2021 *Environ. Eng. Manage. J.* **20** 973.
61. Trifi I M, Chaabane L, Dammak L, Baklouti L and Hamrouni B 2021 *Membranes* **11** 731.
62. Mahdy S A, Raheed Q J and Kalaichelvan P T 2012 *Int. J. Mod Eng Res.* **2** 578.
63. Tran N, Mir A, Mallik D, Sinha A, Nayar S and Webster T J 2010 *Int. J. Nanomed* **5** 277.
64. Kim D K, Zhang Y, Kehr J, Klason T, Bjelke B and Muhammed M 2001 *J. Magn. Magn. Mater.* **225** 256.